Princeton Plasma Physics Laboratory

PPPL-5138

Investigation of ion and electron heat transport of high-T_e ECH heated discharges in the Large Helical Device

N.A. Pablant, S. Satake, M. Yokoyama, D.A. Gates, M. Bitter, N. Bertelli, L. Delgado-Aparicio, A. Dinklage, M. Goto, K.W. Hill, S. Igamai, S. Kubo, S. Lazerson, S. Matsuoka, D.R. Mikkelsen, S. Morita, T. Oishi, R. Seki, T. Shimozuma, C. Suzuki, Y. Suzuki, H. Takahashi, H. Yamada, Y. Yoshimura, and the LHD Experiment Group

July 2015

Prepared for the U.S. Department of Energy under Contract DE-AC02-09CH11466.

Princeton Plasma Physics Laboratory
Report Disclaimers

Full Legal Disclaimer

This report was prepared as an account of work sponsored by an agency of the United States Government. Neither the United States Government nor any agency thereof, nor any of their employees, nor any of their contractors, subcontractors or their employees, makes any warranty, express or implied, or assumes any legal liability or responsibility for the accuracy, completeness, or any third party's use or the results of such use of any information, apparatus, product, or process disclosed, or represents that its use would not infringe privately owned rights. Reference herein to any specific commercial product, process, or service by trade name, trademark, manufacturer, or otherwise, does not necessarily constitute or imply its endorsement, recommendation, or favoring by the United States Government or any agency thereof or its contractors or subcontractors. The views and opinions of authors expressed herein do not necessarily state or reflect those of the United States Government or any agency thereof.

Trademark Disclaimer

Reference herein to any specific commercial product, process, or service by trade name, trademark, manufacturer, or otherwise, does not necessarily constitute or imply its endorsement, recommendation, or favoring by the United States Government or any agency thereof or its contractors or subcontractors.

PPPL Report Availability

Princeton Plasma Physics Laboratory:

http://www.pppl.gov/techreports.cfm

Office of Scientific and Technical Information (OSTI):

http://www.osti.gov/scitech/

Related Links:

U.S. Department of Energy

U.S. Department of Energy Office of Science

U.S. Department of Energy Office of Fusion Energy Sciences

Investigation of ion and electron heat transport of high-T_e ECH heated discharges in the Large Helical Device

N.A. Pablant,[1] S. Satake,[2,3] M. Yokoyama,[2,3] D.A. Gates,[1] M. Bitter,[1] N. Bertelli,[1] L. Delgado-Aparicio,[1] A. Dinklage,[4] M. Goto,[2] K.W. Hill,[1] S. Igamai,[2] S. Kubo,[2] S. Lazerson,[1] S. Matsuoka,[5] D.R. Mikkelsen,[1] S. Morita,[2,3] T. Oishi,[2,3] R. Seki,[2] T. Shimozuma,[2] C. Suzuki,[2] Y. Suzuki,[2,3] H. Takahashi,[2] H. Yamada,[2,3] Y. Yoshimura,[2] and the LHD Experiment Group

[1)] *Princeton Plasma Physics Laboratory, Princeton, New Jersey 08543, USA*

[2)] *National Institute for Fusion Science, Toki, Gifu 509-5292, Japan*

[3)] *SOKENDAI (The Graduate University for Advanced Studies), Toki, Gifu 509-5292 Japan*

[4)] *Max-Planck-Institut für Plasmaphysik, Greifswald, Germany*

[5)] *Research Organization for Information Science and Technology, Kobe, Hyogo 650-0047, Japan*

(Dated: 14 April 2015)

An analysis of the radial electric field and heat transport, both for ions and electrons, is presented for high-T_e electron cyclotron heated (ECH) discharges on the Large Helical Device (LHD). Transport analysis is done using the TASK-3D transport suite[1] utilizing experimentally measured profiles for both ions and electrons. Ion temperature and poloidal rotation profiles are measured using the recently installed x-ray imaging crystal spectrometer diagnostic (XICS)[2], while electron temperature and density profiles are measured using Thomson scattering. The analysis also includes calculated ECH power deposition profiles as determined through the TRAVIS ray-tracing code. This is the first time on LHD that this type of integrated transport analysis with measured ion temperature profiles has been performed without NBI injection, allowing the heat transport properties of plasmas with only ECH heating to be more clearly examined. For this study, a plasma discharge is chosen which develops a high central electron temperature ($T_{eo} = 9keV$) at moderately low densities ($n_{eo} = 1.5 \times 10^{19} m^{-3}$). The experimentally determined transport properties from TASK-3D are compared to neoclassical predictions as calculated by the GSRAKE and FORTEC-3D codes. Predictions of a strong positive neoclassical ambipolar electric field (E_r) in the plasma core are compared to poloidal rotation measurements from the XICS diagnostic. Both the new diagnostic capabilities (XICS) and the integrated modeling help to provide a better understanding of the interplay of transport and the radial electric field in the formation of high temperature electron heated stellarator/heliotron plasmas at low collisionalities.

I. INTRODUCTION

In stellarator plasmas, it is possible to develop plasmas with high central electron temperatures in low collisionality plasmas through the use of electron cyclotron heating (ECH)[3]. These conditions are associated with core electron-root confinement (CERC) plasmas[4], which develop a region of positive electric field and reduced electron heat transport in the central region of the plasma. The core electron-root formation is due to a 3D-specific bifurcation of the ambipolarity condition at low collisionalities. This reduction in transport leads to a peaking of the electron temperature in the core and is known as the high-T_e regime. Plasmas of this type on the Large Helical Device (LHD) have reached central temperatures of greater than $15keV$ in low density conditions, $n_{eo} = 0.2 \times 10^{19} m^{-3}$, and greater than $9keV$ even with densities as high as $n_{eo} = 1.5 \times 10^{19} m^{-3}$.

In these plasmas, neoclassical predictions based on the condition of ambipolar flows predict a positive electric field (electron-root solution) across the core region of the plasma when in the high-T_e regime, while a negative electric field is otherwise expected. Previous studies have reported that a transition from the ion-root phase to the electron-root phase requires a particular ratio of density to input power. An understanding of the applicability of the neoclassical predictions to these plasmas, as well as the dynamics involved in developing the electron root region, is being actively pursued at LHD.[5–9]

In this paper high-T_e plasmas are revisited by looking at the detailed evolution of a CERC discharge which is produced using only ECH heating. In the discharge studied, an increase in power and decrease in density is associated with an expansion of the positive radial electric field from a well defined core region to a region covering the majority of the plasma minor radius. The associated changes in transport brought about by this transition will also be examined.

The analysis of the transport and radial electric field structure is performed with the TASK3D transport suite along with measurements of the poloidal rotation from the high resolution x-ray crystal spectrometer (XICS)[2]. For this analysis the ion temperature profiles are taken from the XICS system, and electron temperature profiles are taken from the Thomson scattering system[10]. To determine the ECH heat deposition profile the TRAVIS ray-tracing code[11] is used. Heat transport estimates will be made using power balance considerations based on the plasma parameters and calculated power deposition profiles. Finally, the experimental estimates of the ion and electron heat fluxes and the radial electric field will be compared with neoclassical predictions.

This work benefits from the recent installation of the XICS diagnostic which allows, for the first time on LHD,

the ion heat transport and poloidal rotation to be measured in the absence of any neutral beam injection. This enables the study of plasmas that are only heated using ECH. The use of a single source of external heating simplifies power balance calculations and reduces the sources of uncertainties. In addition, neoclassical calculations or simulations of a plasma without momentum input by NBI are significantly easier to perform, and in most neoclassical treatments external momentum drive is neglected. The neoclassical calculations in the current work are more directly comparable with the experimental values since no external momentum input sources are present during the shot evolution.

The analysis developed for this study highlights the current capabilities of the TASK-3D suite for thermal transport analysis and demonstrates the integration of a set of equilibrium and power deposition codes, providing the base set of tools required for power balance analysis in stellarator geometries.

II. METHODS

A. Shot Evolution

The analysis in this paper is based around an ECH heated discharge from the 16th LHD experimental campaign in 2012. Time traces for shot 114722, are shown in Fig.1. This discharge begins as a typical CERC plasma with a transition from a low-T_e phase to high-T_e phase as the ECH heating power is increased. Typical density and temperature profiles during these two phases are shown in Fig.2.

This discharge utilizes an inward shifted configuration with the magnetic axis location set to 3.53m. The magnetic field on axis is +2.705T, which corresponds to the clockwise direction when viewed from the top. During most of this shot, only ECH heating is used, with a peak injected power of $4.4MW$. This heating is achieved using a combination of the three $77GHz$, one $82.7GHz$ and one $154GHz$ systems, and is injected from multiple launcher systems[12].

Starting at $3.5s$ the 154GHz Gyrotron is turned on increasing the injected power from $2.5MW$ to $3.4MW$. An additional $77GHz$ system is added at 3.64 seconds raising the injected power to $4.4MW$. During the $200ms$ after the power increase at 3.5 seconds, the plasma transitions from a low-T_e phase to a high-T_e phase. During this transition it can be observed that the line integrated density decreases (from $1.6\times10^{19}m^{-3}$ to $1.0\times10^{19}m^{-3}$), the electron temperature increases (from $4keV$ to $9keV$), and there is a dramatic change in poloidal rotation. While the electron temperature increases dramatically, the density loss and reduction in T_i leads to an overall reduction in the total stored energy, a relatively constant electron stored energy, and a strong decrease in the ion stored energy (see Fig.1(b)). During this shot, and in particular around the transition time, there is no significant change in the gas puffing rate or any other particle fueling source (except during neutral beam injection).

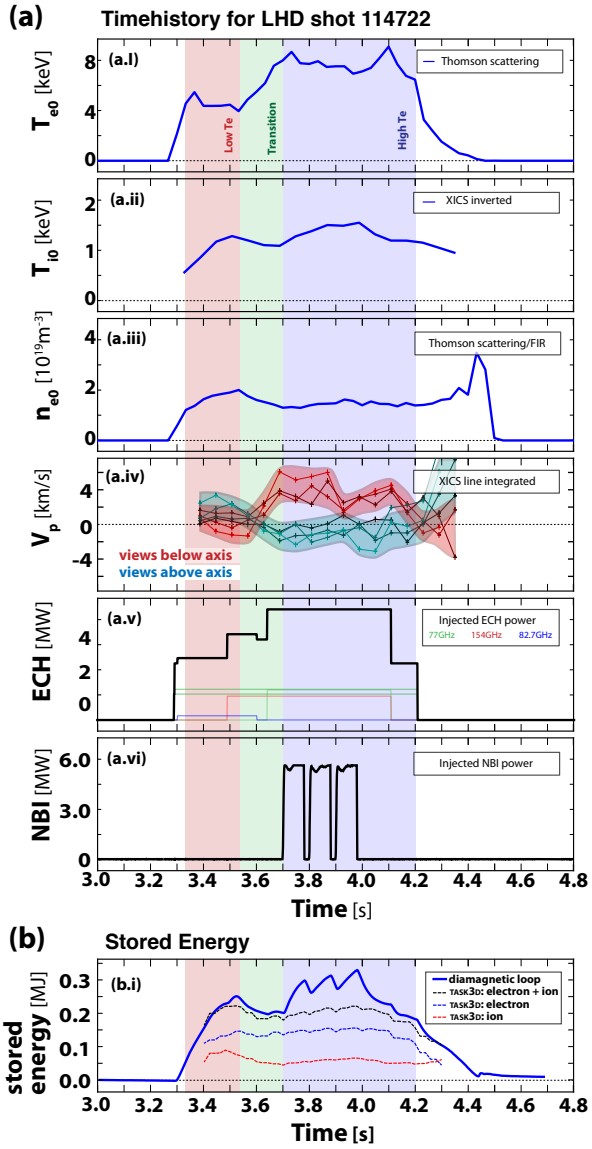

FIG. 1. (a) Time evolution of LHD shot 114722. (a.i) Central electron temperature as measured by Thomson scattering and averaged over the 10 central channels. (a.ii) Inverted central ion temperature from the XICS diagnostic. (a.iii) Central electron density taken from Thomson scattering and normalized to the line integrated measurements from the FIR system. (a.iv) Line integrated poloidal rotation, measured by the XICS diagnostic. (a.v) Injected ECH power. The black line represents the total injected power, the colored lines represent individual gyrotrons. (a.vi) Injected NBI power from the perpendicular neutral beam. (b) Time history of the plasma stored energy. The solid blue line is the total stored energy as measured by the diamagnetic loop. The blue and red dashed lines represent kinetic stored energy calculated from the measured temperature and density profiles. The black dashed line shows the total kinetic stored energy found by adding the ion and electron stored energy.

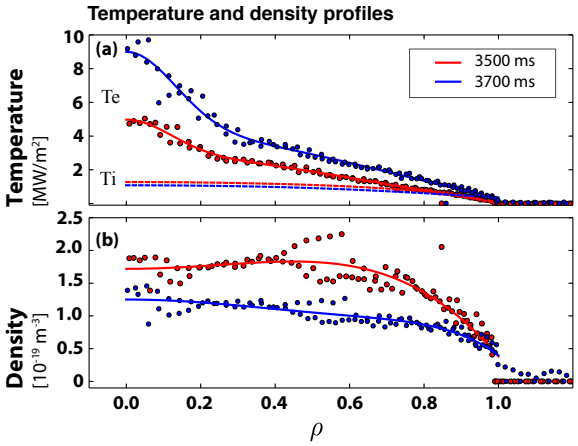

FIG. 2. Temperature and density profiles for 114722 at $3500ms$ and $4000ms$. (a) Electron temperature from the Thomson scattering and inverted ion temperature from the XICS system. (b) Electron density found from Thomson scattering and normalized to the line integrated density reported by the far infrared laser interferometer system (FIR). In all plots the points represent the raw data, and the solid lines represent the fit to the data used in the analysis.

During the time between 3.7 and $4.0s$, $5.4MW$ of port-through injected neutral beam power is added by one of the $40keV$ perpendicular neutral beams (NBI #5). In the current analysis we focus on the plasma state before the NBI turn on ($3.7s$) and after the NBI turn off and subsequent relaxation of the fast ion distribution ($4.1s$), and therefore do not include the NBI deposition in the calculations.

Correlated with the increase of the central electron temperature after 3.5s is a dramatic change in the argon poloidal rotation, as measured by the XICS system. The time evolution of the line integrated poloidal velocity measurements can be seen in Fig.1(a.iv). The detailed rotation profiles, shown in Fig.3, indicate that during the low-T_e phase there is a core region of the plasma rotating in the negative poloidal direction (ion-diamagnetic drift direction), while the outer portion of the plasma is rotating in the positive direction. During the transition phase, the rotation inversion radius expands outward, and in the high-T_e phase the entire central plasma (the measurement range is limited to $\rho \leq 0.8$) is rotating in the negative direction. The poloidal rotation and electric field are closely related, and a negative poloidal plasma rotation corresponds to a positive radial electric field, as described in Section III.

B. TASK3D

The TASK3D suite has been developed to provide an integrated package for power balance analysis on LHD.[1,13,14] It acts as a framework to integrate multiple codes and calculations, and to provide the necessary data gathering and manipulation to consistently enable transport analysis for 3D geometries. There are numerous modules that can be included as part of the TASK3D framework, however for the current work only a subset of available calculations will be used.

For these initial studies a simplified transport model is used that only considers ECH power deposition, local collisional temperature equilibration between electrons and the main ions (hydrogen), time evolution of the temperature and density profiles, and the heat transport across flux surfaces. Some significant simplifications will be used such as assuming $n_e = n_i$ across the entire profile, and neglecting any radiative losses.

For the analysis done in this paper, PYTASK3D was developed as a alternative front end for the TASK3D suite. This package handles preparation of the diagnostic profiles and integration of the analysis modules. The development of PYTASK3D was done as part of a collaborative effort between NIFS and PPPL.

C. Diagnostic Profiles

In order to carry out the transport analysis, accurate measurement of the ion and electron temperature profiles are required. The XICS diagnostic, installed in 2011 and upgraded in 2012, allows, for the first time on LHD, for full ion temperature profiles to be measured in the absence of neutral beam injection.

The XICS diagnostic provides line integrated measurements of the plasma ion temperature and poloidal rotation profile. These line-integrated measurements are then inverted, using tomographic inversion techniques, to recover the true temperature and rotation profiles as a function of the flux coordinate. This inversion process assumes that the argon emissivity and temperature are constant on flux surfaces. A smooth spline representation for the final ion temperature is enforced as part of the inversion process used for the XICS profiles. The details of the diagnostic operation and inversion techniques are described in Ref. 2,15.

Electron temperature profiles are measured by the Thomson scattering system[10]. For the electron density the profile measured by Thomson scattering is normalized to match the line integrated density measured by the Far Infrared Reflectometer (FIR) system[16]. The temperature and density profiles are then filtered to remove bad channels based on median filtering of the time history of each channel.

Before using any of the diagnostic data in the transport calculations, the profiles are fitted using a smooth function. Several profile representations are implemented in TASK3D which can be used to fit the raw diagnostic data. The choice of the profile representation forces a structure onto profiles which affects the detailed calculations of the diffusion coefficients. While the overall conclusions from this analysis do not depend on the profile fitting function, the detailed shape of the diffusion co-

efficient profiles vary slightly depending on which representation is used. The two profile shapes that have been compared in the course of this analysis are a Gaussian plus polynomial representation and a cubic spline representation. The results shown in this paper are based on the fits shown in Fig.2. Fitting against $\rho = \sqrt{\phi/\phi_{edge}}$ is done using a Gaussian plus polynomial representation with a sixth degree even polynomial. In the current work the uncertainties in the measurements of T_e and n_e are not well characterized, and therefore the profiles are fit without weighting ($\chi^2 \sim \sum(m_i - f)^2$). For T_i and V_p, the profiles are found through a tomographic inversion algorithm which takes into account both experimental and algorithmic uncertainties.[15]

Since the ion temperature used in the current analysis is based on measurement of the argon temperature, it is important to consider whether thermal equilibration with the main ions (hydrogen) can be expected. A simple 3 species transport model (hydrogen, carbon, argon) has been constructed that confirms that the impurity temperatures are expected to closely match the hydrogen temperatures for the conditions in this plasma shot.

D. Equilibrium reconstruction

A reconstruction of the 3D plasma equilibrium is required as part of the TASK3D analysis for both calculations of the plasma volume and shape, as well as for the mapping of the various diagnostic measurement locations to a effective minor radius. This same equilibrium is also used to invert the line-integrated XICS measurements and determine the local ion temperature and rotation profiles.[15]

The standard approach in stellarators and heliotrons is to model the plasma equilibrium as a set of nested flux surfaces through the use of the VMEC code[17]. The assumption of nested flux surfaces provides a good model for the equilibrium over most of the plasma volume. In the plasma edge, the true plasma equilibrium is expected to become stochastic, however the general plasma shape is still reasonably approximated by the VMEC model.

The VMEC code produces an equilibrium based on a set of fixed inputs. To find an equilibrium that matches a particular plasma, a reconstruction technique is needed. For the current work the STELLOPT reconstruction tool was used for equilibrium reconstruction. STELLOPT uses a minimization technique to determine a VMEC equilibrium that best matches the available diagnostic data.[18,19]. This is done by optimizing the pressure profile, toroidal current profile, total enclosed toroidal flux and a pressure scaling factor that are used in a free boundary VMEC equilibrium calculation. For the current reconstructions, the following measurements were targeted: flux loop measurements, electron temperature profile, electron density profile, total stored energy, and total toroidal current.

E. Power deposition and profile evolution

Our final transport estimates are based on a power balance calculation that includes only the ECH power deposition and the collisional thermal equilibration between electrons and the main ion (hydrogen).[20] The time dependent evolution of the ion and electron stored energy (profile evolution) is available for inclusion as part of the TASK3D, however due to the lack of time resolution and uncertainties in the diagnostic profiles this is not included in the current calculation. No other sources of power deposition or loss are considered in this current analysis. The calculated heat deposition, thermal equilibration and stored energy evolution profiles are shown in Fig.4.

In the current version of TASK3D the time dependent stored energy evolution is handled by creating an effective power deposition profile that takes into account the change in the temperature and density profiles. This profile evolution profile is found using simple differences between adjacent fitted profiles. For the electron heat flux, the profile evolution has a negligible effect compared to the ECH power deposition, which provides the plasma with an order of magnitude more power. For the ion heat flux the change in the stored energy is on the order of the electron-ion heat transfer, and therefore may play a more significant role. The profile evolution is nonetheless neglected in the current analysis due to the difficulty of making an accurate estimation given that the diagnostic time resolution is similar to the shot evolution timescale. The inclusion of the stored energy evolution would add a great deal of uncertainty and make drawing conclusions from the ion power balance calculation difficult. For the current analysis an assumption is made that only small changes in the ion stored energy would be expected between $3700ms$ and $4100ms$ if it were not for the introduction of the neutral beam, and therefore the evolution of the ion stored energy can be neglected. Such an assumption is at least consistent with the time history of the kinetic stored energy, shown in Fig.1(b).

Calculation of the ECH deposition profile has been done using ray-tracing techniques. There are two available ray-tracing codes that have been used for this calculation: TRAVIS[11] and LHDGAUSS[21,22]. TRAVIS is a generalized code for electron cyclotron propagation in 3D geometry, and has been applied to several stellarator systems. The LHDGAUSS code has been specifically developed at NIFS for LHD plasmas. Both codes use a VMEC geometry description and fitted T_e and n_e profiles as the inputs. Separate ray-tracing runs are performed for each combination of launcher, frequency and propagation mode active in the plasma, and then combined based on the expected input power in each case.

Results from the TRAVIS are shown in Fig.4. The results from LHDGAUSS show a qualitatively similar deposition profile, giving us confidence is the accuracy of the calculation implementations. The major uncertainty in these calculated deposition profiles stems from the den-

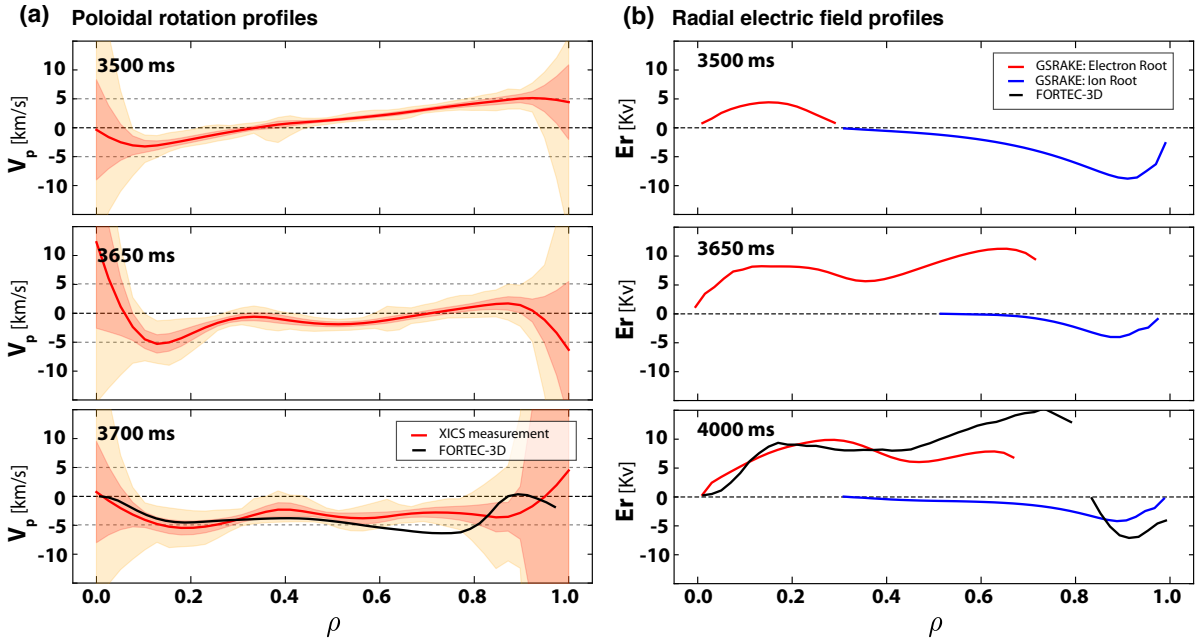

FIG. 3. (a) Argon poloidal rotation profiles as measured by the XICS diagnostic. Profiles are found through tomographic inversion of the line integrated spectral measurements. Shaded regions represent the approximate error in the final inverted profile due to photon statistics. The red shaded region represents the standard deviation, while the yellow region represents the extreme solutions consistent with the measurements. (b) Radial electric field profiles as calculated by GSRAKE. The red line represents the electron root solution, the blue line represents the ion root solution, the unstable solution is not displayed. Solutions for the radial electric field and main ion poloidal rotation as calculated by FORTEC-3D are shown for the high-T_e phase by the black line.

sity profile in the plasma edge. Sufficiently accurate density profiles are not available in this region, requiring extrapolation from Thomson density profile as shown in Fig.2. This lack of information in the edge affects the calculation of the mode fractions (X or O mode) that enter the plasma. The approximation used in the current calculation is that all of the injected power is coupled into the targeted mode. The other major approximation is that only first pass absorption is considered, and the total absorbed power is normalized to the injected power. The ray tracing results show that most of the power is absorbed on the first pass and that this approximation should have a small effect on the accuracy of the results in this case.

During this shot, one of the perpendicular neutral beams is turned on from $3.7s$ to $4.0s$, during the high-T_e period. This $40keV$ neutral hydrogen beam injects approximately $5.4MW$ of port-through power. Inclusion of the NBI in the power balance calculation is possible, but accurate calculations are difficult and require not only the calculation of the initial deposition of fast ions, but also fast ion slowing down, fast ion loss, and electron cooling due to particle fueling. For these reasons we limit our analysis to $3.7s$, before the neutral beam turn on, and $4.1s$ after the neutral beam turn off and subsequent slowing down time. The slowing down time, combined with the fast ion confinement time, can be seen experimentally in the stored energy measurements shown in Fig.1(b) after the neutral beam is turned off at $4.0s$.

F. neoclassical predictions

One of the goals of this analysis is to compare experimentally determined heat fluxes and poloidal rotation profiles with neoclassical predictions, there by gaining some insight into the both the validity of the neoclassical calculation and the amount of transport that can be attributed to neoclassical effects. Neoclassical predictions have been calculated by both the GSRAKE code (see Ref. 23,24) and the FORTEC-3D code (see Ref. 25,26). Both of these codes find the radial electric field (E_r) required to achieve an ambipolar particle flux in stellarator geometries. The predicted neoclassical radial electric field and predicted heat flux from these codes is shown in Fig.3 and Fig.5 respectively. When comparing these neoclassical predictions to experimental quantities, it is important to note that neither GSRAKE or FORTEC-3D include impurity species (such as argon) in any of the calculations.

The GSRAKE code is based on a general solution of the ripple-averaged kinetic equation. This treatment is valid only in the case of simple stellarator geometry, of which LHD qualifies. Details on the applicability of GSRAKE to LHD, and comparisons against other calculation techniques are detailed in Ref. 27.

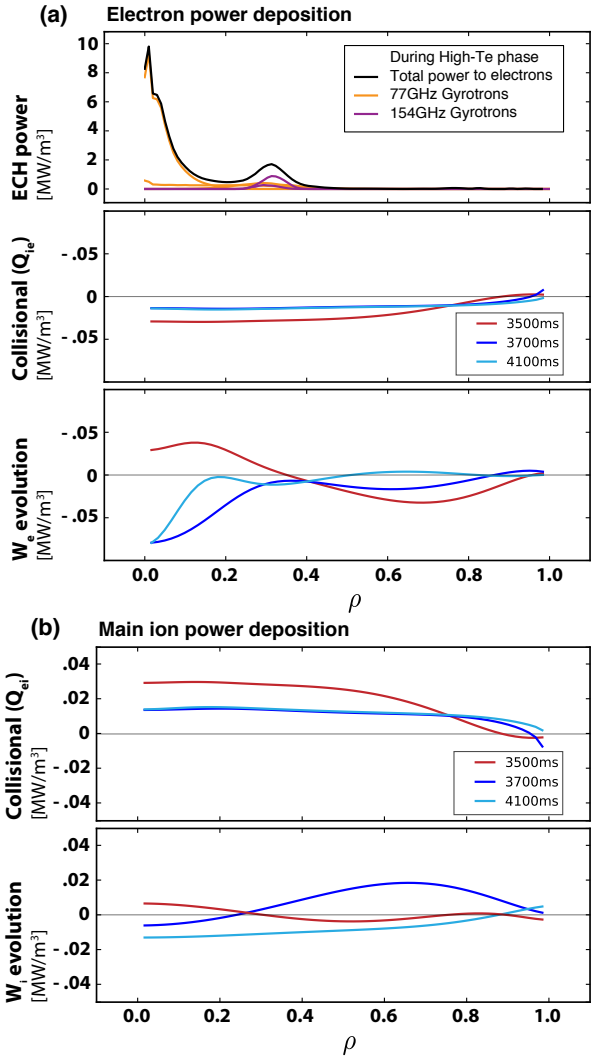

FIG. 4. Power deposition profiles for LHD shot 114722 calculated for electrons (a), and main ions (b). Profiles for ECH deposition, electron-ion coupling and time dependent stored energy evolution are shown. The stored energy evolution profiles are shown here for comparison with the other power deposition profiles but are not included in the final power balance calculation. ECH deposition is calculated using the TRAVIS ECH ray-tracing code and includes the three 77GHz and the 154GHz systems. The ECH deposition profiles are only shown for the high-T_e phase; the low-T_e deposition profile is similar but not as strongly peaked on axis.

FORTEC-3D uses a Monte-Carlo particle following approach, allowing it to use fewer assumptions and account for non-local finite orbit effects. For the results shown in this work, a new technique was used that allowed FORTEC-3D to calculate both the ion and electron particle fluxes for a self consistent solution for the radial electric field and other neoclassical transport parameters. This calculation is done by first calculating a guess of the radial electric field E_{r0} using a local code for the electron fluxes and FORTEC-3D for the ion particle fluxes. The initial guess is obtained by solving the time evolution of E_r according to the radial current, $dE_r/dt = -\frac{e}{\epsilon_\perp \epsilon_0}(Z_i\Gamma_I - \Gamma_e)$, where Γ denotes the particle fluxes and $\epsilon_\perp$ denotes the effect of the classical polarization current (see Ref. 9). A series of E_r profiles are then created based on this initial guess, $E_{r0} \pm \Delta E$, and FORTEC-3D is run on each E_r profile in this series to calculate both ion and electron fluxes. This provides the dependence of the particle flux as a function of E_r at each point in the plasma. Finally the ambipolar solution is found by fitting the E_r dependence of the difference in particle fluxes $(Z_I\Gamma_I - \Gamma_e)$ and finding the zero crossing. Compared to a local neoclassical solution like GSRAKE, this method importantly includes the higher-order effects such as the ion finite-orbit-width and E_r-shear on the neoclassical flux. In the FORTEC-3D results shown in Fig.3, the calculation between $\rho = 0.75$ and $\rho = 0.85$ has a high uncertainty because the particle fluxes calculated by FORTEC-3D become insensitive to the radial electric field in this region.

III. RESULTS

The power balance analysis of this discharge focuses on three times, $3500ms$, $3700ms$ and $4100ms$. The first time is during the low-T_e phase, while the later two times are both in the high-T_e phase, before and after the NBI injection (as described in Section II E). For the analysis of both the low-T_e and high-T_e cases, the plasma has not completely reached a steady state in terms of the electron temperature and density profiles, however the stored energy evolution terms have been examined and are have a small effect on the electron power balance. More importantly, the poloidal rotation profile is fully evolved giving confidence that the results capture the essential transport properties at the analysis times.

The power balance calculations performed using TASK3D assume thermalized electron and ion distributions at the chosen analysis times (when the neutral beams are not active). This assumption is supported by the close agreement between the kinetic energy, calculated using the measured temperature and density profile, and the stored energy measured by the diamagnetic loop (see Fig.1(b)). This agreement provides confidence that at the analysis times there are no fast ion or fast electron populations that need to be considered, and that the argon and hydrogen temperatures are the same.

The ion and electron heat flux calculated by TASK3D are shown in Fig.5, and compared with neoclassical predictions from GSRAKE. Both the electron root and the ion root solutions from GSRAKE are shown. The poloidal rotation measurements shown in Fig.3 can be used to determine that during the high-T_e the electron root solution should be chosen wherever two solutions exist. This choice is also supported by the agreement between in the ion heat flux between the power balance analysis and the neoclassical electron root solution; the ion root solution, with $Q_{\mathrm{Neoclassical}} > Q_{\mathrm{PowerBalance}}$, is not physically real-

istic.

For the ions, the experimental heat fluxes are approximately the same as the neoclassical predictions over most of the plasma (when choosing the electron root solution). This suggests that the ion flux is dominated by neoclassical effects. As mentioned in Section II E, the stored energy time evolution was not included in the power balance measurement. This adds uncertainty to the quantitative comparison between the power balance and neoclassical calculations, however the qualitative agreement is captured by the current results.

For the electrons the neoclassical electron heat flux is nearly an order of magnitude lower than the measured heat flux in both the low and high T_e phases. This is an indication that electron transport is almost entirely dominated by turbulent sources in the range $0.3 < \rho < 0.8$ where power balance and neoclassical calculations are available without large uncertainties. After the transition to the high-T_e phase, an increase in the electron heat flux is seen in both the neoclassical and experimental heat fluxes, however because of the uncertainties in both calculations it is not possible to draw strong conclusions about the source of this increase, weather neoclassical or turbulent.

Calculation of the thermal diffusion coefficients during the low-T_e and high-T_e phases are shown in Fig.6. Even before entering the high-T_e phase, the electron thermal diffusion coefficient, χ_e shows a region of reduced transport inside of $\rho = 0.4$. During the high-T_e phase, this reduced transport region is maintained, while outside of this region the transport is increased. This behavior can be seen in the electron temperature profile where the temperature and temperature gradient increase dramatically inside of $\rho = 0.4$, but change more modestly outside of this region. The majority of the electron heating is deposited in the core region of the plasma.

The ion temperature decreases only slightly between the low and high T_e phases. Without neutral beam injection, the only power being deposited to the ions is from electron-ion collisional thermal transfer. This transfer has a dependency on the electron temperature that goes as approximately $n_e^2 T_e^{-1/2}$, when $T_i << T_e$ as in the present case, and therefore there is less heating of the ions as the electron temperature increases and density decreases (see Fig.4). Since there are only small changes in the ion temperature, or ion temperature gradient, this is seen as a reduction in the ion thermal diffusion coefficient, χ_i.

Measurements of the poloidal rotation can give us some insight into how the radial electric field changes during the transition to the high-T_e phase. The poloidal rotation can be related to the radial electric field through the force balance equation[28–30].

$$E_r = \frac{1}{e n_I Z_I}\frac{\partial p_I}{\partial r} - (v_\theta B_\phi - v_\phi B_\theta) \qquad (1)$$

where r is in a direction perpendicular to the magnetic flux surface, the subscript I denotes the ion species, n_I is the ion density, Z_I is the charge, p_I is the pressure, v is the velocity, and B is the magnetic field. The pressure gradient and toroidal velocity terms are typically quite small in stellarator plasmas, especially in the case of argon which has a large value of Z. This allows us to relate, qualitatively, the radial electric field profile directly to the measurement of the poloidal rotation. The poloidal rotation measurements, taken from the XICS system, show an expansion of the electron root region from the core region inside of $\rho = 0.3$ (low-T_e phase) to the entire plasma out to $\rho \geq 0.8$ (high-T_e phase), see Fig.3.

These measurements are consistent with the neoclassical calculations of E_r from GSRAKE and FORTEC-3D. Inside of $\rho = 0.3$ GSRAKE finds a single electron root solution, with a positive radial electric field, to exist for both the low-T_e and high-T_e phases of this shot. During the low-T_e phase, GSRAKE only finds a single ion root solution outside of $\rho = 0.3$, with a small negative E_r. After the transition to the high-T_e phase an electron root solution, with a large positive E_r, is also found as a possible solution over most of the core plasma, out to approximately $\rho = 0.7$. Similarly FORTEC-3D predicts an electron root solution out to $\rho = 0.8$, which is in general agreement with the rotation measurements.

A direct quantitative comparison of the measured and neoclassical poloidal rotation is not possible in the current work since the measured rotation is for argon, while the neoclassical calculation is done only considering hydrogen (but assuming that the hydrogen temperature profile is equal to the argon temperature). It is possible however to see a qualitative agreement in the shape of the rotation profile and the magnitude of the rotation velocity, as shown for the FORTEC-3D calculation in Fig.3.

IV. CONCLUSION

A detailed study has been completed of a high-T_e ECH heated discharge which transitions from a state with a localized core electron-root E_r, to a global electron-root E_r, with a corresponding increase in the central electron temperature. The use of the XICS diagnostic along with the TASK3D suite has allowed the radial electric field structure to be inferred, as well as the both the ion and electron heat transport.

The current results are consistent with the results from NBI sustained plasmas with ECH heating, such as in-Ref. 8 and Ref. 7. The final determined central value for the electron thermal diffusion coefficient during the high-T_e phase is similar between the these studies. Previous studies however have focused on the electron transport properties, and have not reported ion heat transport results. The current results for both the heat transport and radial electric field structure in the absence of NBI injection contribute to the general understanding of CERC discharges as well as the role of the neutral beams in these previous studies.

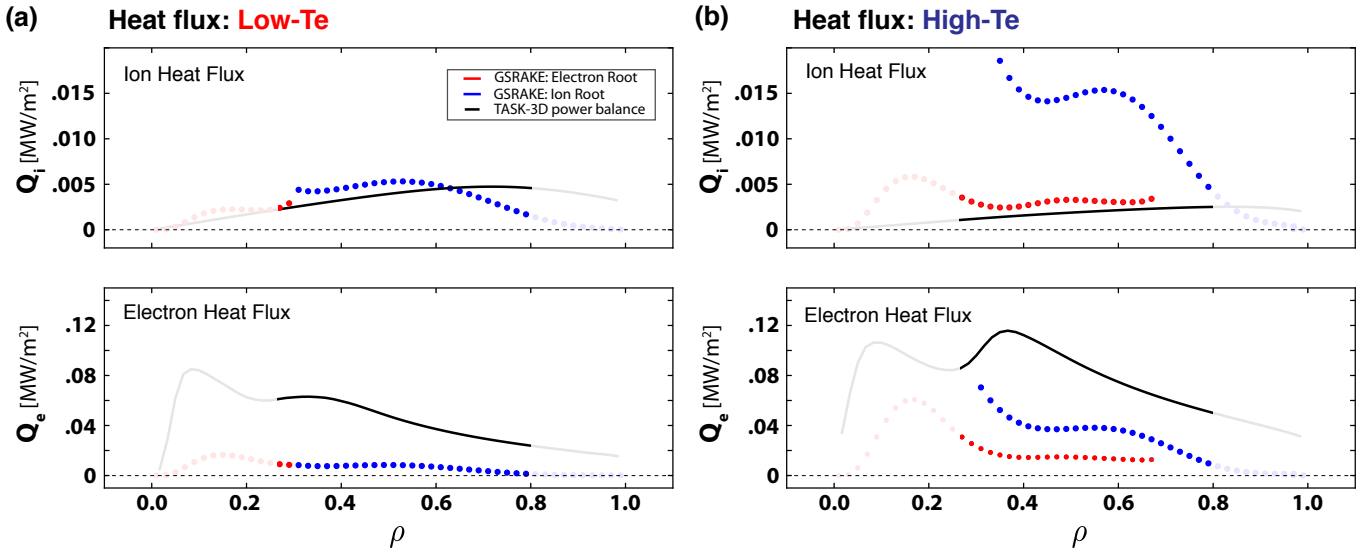

FIG. 5. Transport analysis showing ion and electron heat fluxes during the low-T_e and high-T_e phases of shot 114722. The black line shows TASK3D power balance calculations. The red points represent the GSRAKE neoclassical electron-root solution, while the blue points represent the ion-root solution; the unstable solution is not shown. The low-T_e plots use profiles from $3500ms$, the high-T_e plots use profiles $3700ms$ for the power balance results and $4000ms$ for the neoclassical calculation. There are large uncertainties in the profiles and flux surface geometry for $\rho < 0.3$ and $\rho > 0.8$, therefore these regions have been deemphasized.

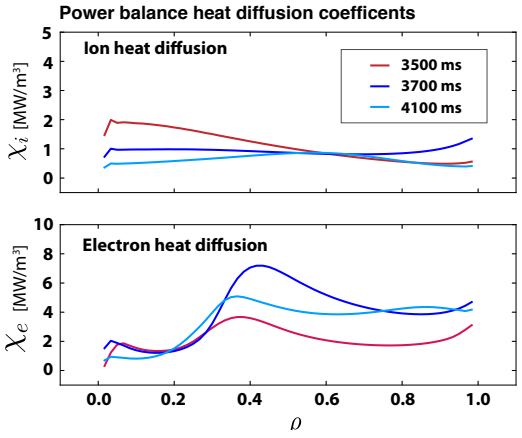

FIG. 6. Thermal diffusion coefficients for ions and electrons calculated for 114722 at $3500ms$, $3700ms$ and $4100ms$ as determined from power balance.

Measurements of the poloidal rotation show qualitatively good agreement with neoclassical calculations of the radial electric field from FORTEC-3D and GSRAKE both in the low-T_e and high-T_e phases of this shot. This gives additional confidence to previously reported results for high-T_e plasmas with only ECH heating, such as in Ref. 9, as well as confidence in future studies using these software tools. Future studies will allow this evolution to be more carefully measured and provide more direct theoretical comparisons.

Finally the current capabilities of the TASK3D suite for use in stellarator/heliotron transport research have been highlighted. This framework will be used for future transport studies to build further understanding of stellarator plasmas and the role of neoclassical transport.

Research supported by the U.S. DOE under Contract No. DE-AC02-09CH11466 with Princeton University. Development of TASK3D is supported by NIFS collaborative Research Programs NIFS14KNTT025. Part of simulations have been carried out on Plasma Simulator in NIFS under the support by NIFS collaborative Research Programs NIFS13KNST051.

[1]M. YOKOYAMA, C. SUZUKI, R. SEKI, M. OSAKABE, M. YOSHINUMA, M. SATO, A. WAKASA, S. MURAKAMI, A. FUKUYAMA, Y. SUZUKI, K. IDA, H. LEE, and the LHD experiment group, Plasma and Fusion Research **8**, 2403016 (2013).
[2]N. A. Pablant, M. Bitter, L. Delgado-Aparicio, M. Goto, K. Hill, S. Lazerson, S. Morita, A. Roquemore, D. Gates, D. Monticello, G. H. Nielson, A. Reiman, M. Reinke, J. Rice, and H. Yamada, Review of Scientific Instruments **83**, 083506 (2012).
[3]M. Yokoyama, H. Maaßberg, C. Beidler, V. Tribaldos, K. Ida, T. Estrada, F. Castejon, A. Fujisawa, T. Minami, T. Shimozuma, Y. Takeiri, A. Dinklage, S. Murakami, and H. Yamada, Nuclear Fusion **47**, 1213 (2007).
[4]M.Yokoyama, O.Yamagishi, K.Ida, M.Yoshinuma, Y.Takeiri, S.Morita, H.Funaba, K.Nagaoka, O. Kaneko, and the LHD Experimental Group, Proceedings of the 17th International Toki Conference , P1 (2007).
[5]Y. Takeiri, T. Shimozuma, S. Kubo, S. Morita, M. Osakabe, O. Kaneko, K. Tsumori, Y. Oka, K. Ikeda, K. Nagaoka, N. Ohyabu, K. Ida, M. Yokoyama, J. Miyazawa, M. Goto, K. Narihara, I. Yamada, H. Idei, Y. Yoshimura, N. Ashikawa, M. Emoto, H. Funaba, S. Inagaki, M. Isobe, K. Kawahata, K. Khlopenkov, T. Kobuchi, A. Komori, A. Kostrioukov, R. Kumazawa, Y. Liang, S. Masuzaki, T. Minami, T. Morisaki, S. Murakami, S. Muto, T. Mutoh, Y. Nagayama, Y. Nakamura, H. Nakanishi, Y. Narushima, K. Nishimura, N. Noda, S. Ohdachi,

T. Ozaki, B. J. Peterson, A. Sagara, K. Saito, S. Sakakibara, R. Sakamoto, M. Sasao, K. Sato, M. Sato, T. Seki, M. Shoji, H. Suzuki, N. Tamura, K. Tanaka, K. Toi, T. Tokuzawa, K. Y. Watanabe, T. Watari, Y. Xu, H. Yamada, M. Yoshinuma, K. Itoh, K. Ohkubo, T. Satow, S. Sudo, T. Uda, K. Yamazaki, Y. Hamada, K. Matsuoka, O. Motojima, M. Fujiwara, T. Notake, N. Takeuchi, Y. Torii, S. Yamamoto, T. Yamamoto, T. Akiyama, P. Goncharov, T. Saida, H. Kawazome, and H. Nozato, Physics of Plasmas **10**, 1788 (2003).

[6] T. Shimozuma, S. Kubo, H. Idei, Y. Yoshimura, T. Notake, K. Ida, N. Ohyabu, I. Yamada, K. Narihara, S. Inagaki, Y. Nagayama, Y. Takeiri, H. Funaba, S. Muto, K. Tanaka, M. Yokoyama, S. Murakami, M. Osakabe, R. Kumazawa, N. Ashikawa, M. Emoto, M. Goto, K. Ikeda, M. Isobe, T. Kobichi, Y. Liang, S. Masuzaki, T. Minami, J. Miyazawa, S. Morita, T. Morisaki, T. Mutoh, H. Nakanishi, K. Nishimura, N. Noda, S. Ohdachi, Y. Oka, T. Ozaki, B. J. Peterson, Y. Narushima, A. Sagara, K. Saito, S. Sakakibara, R. Sakamoto, M. Sasao, M. Sato, K. Satoh, T. Seki, S. Shoji, H. Suzuki, N. Tamura, K. Tokuzawa, Y. Torii, K. Toi, K. Tsumori, K. Y. Watanabe, T. Watari, S. Yamamoto, T. Yamamoto, M. Yoshinuma, K. Yamazaki, S. Sudo, K. Ohkubo, K. Itoh, A. Komori, H. Yamada, O. Kaneko, Y. Nakamura, K. Kawahata, K. Matsuoka, O. Motojima, and the LHD Experimental Group, Plasma Physics and Controlled Fusion **45**, 1183 (2003).

[7] K. Ida, S. Inagaki, T. Shimozuma, N. Tamura, H. Funaba, K. Narihara, S. Kubo, S. Murakami, A. Wakasa, M. Yokoyama, Y. Takeiri, K. Y. Watanabe, K. Tanaka, M. Yoshinuma, Y. Liang, N. Ohyabu, T. Akiyama, N. Ashikawa, M. Emoto, T. Fujita, T. Fukuda, P. Goncharov, M. Goto, H. Idei, K. Ikeda, A. Isayama, M. Isobe, O. Kaneko, K. Kawahata, H. Kawazome, T. Kobuchi, A. Komori, R. Kumazawa, S. Masuzaki, T. Minami, J. Miyazawa, T. Morisaki, S. Morita, S. Muto, T. Mutoh, Y. Nagayama, Y. Nakamura, H. Nakanishi, Y. Narushima, K. Nishimura, N. Noda, T. Notake, H. Nozato, S. Ohdachi, Y. Oka, S. Okajima, M. Osakabe, T. Ozaki, B. J. Peterson, A. Sagara, T. Saida, K. Saito, S. Sakakibara, R. Sakamoto, Y. Sakamoto, M. Sasao, K. Sato, M. Sato, T. Seki, M. Shoji, H. Suzuki, N. Takeuchi, K. Toi, T. Tokuzawa, Y. Torii, K. Tsumori, T. Watari, H. Yamada, I. Yamada, S. Yamamoto, T. Yamamoto, Y. Yoshimura, K. Itoh, K. Matsuoka, K. Ohkubo, S. Sudo, T. Uda, K. Yamazaki, and O. Motojima, Physics of Plasmas **11**, 2551 (2004).

[8] T. Shimozuma, S. Kubo, H. Idei, S. Inagaki, N. Tamura, T. Tokuzawa, T. Morisaki, K. Watanabe, K. Ida, I. Yamada, K. Narihara, S. Muto, M. Yokoyama, Y. Yoshimura, T. Notake, K. Ohkubo, T. Seki, K. Saito, R. Kumazawa, T. Mutoh, T. Watari, A. Komori, and the LHD Experimental Group, Nuclear Fusion **45**, 1396 (2005).

[9] S. Matsuoka, S. SATAKE, H. TAKAHASHI, A. WAKASA, M. YOKOYAMA, T. IDO, A. SHIMIZU, T. SHIMOZUMA, S. MURAKAMI, and LHD Experiment Group, Plasma and Fusion Research **8**, 1403039 (2013).

[10] I. Yamada, K. Narihara, H. Funaba, T. Minami, H. Hayashi, T. Kohmoto, and L. E. Group, Fusion Science and Technology **58**, 345 (2010).

[11] N. B. MARUSHCHENKO, V. ERCKMANN, H. J. HARTFUSS, M. HIRSCH, H. P. LAQUA, H. MAASSBERG, and Y. TURKIN, Plasma and Fusion Research **2**, S1129 (2007).

[12] T. SHIMOZUMA, H. TAKAHASHI, S. KUBO, Y. YOSHIMURA, H. IGAMI, M. NISHIURA, S. OGASAWARA, R. MAKINO, H. IDEI, N. B. MARUSHCHENKO, Y. TURKIN, and T. MUTOH, Plasma and Fusion Research **8**, 2402073 (2013).

[13] Yokoyama, M. for TASK3D Users and Developers, memo 61 (NIFS, 2012).

[14] A. Wakasa, A. Fukuyama, S. Murakami, M. Miki, M. Yokoyama, M. Sato, S. Toda, H. Funaba, K. Tanaka, K. Ida, H. Yamada, M. Honda, and N. Nakajima, in *23rd IAEA Fusion Energy Conf.* (2010).

[15] N. A. Pablant, R. E. Bell, M. Bitter, L. Delgado-Aparicio, K. W. Hill, S. Lazerson, and S. Morita, Review of Scientific Instruments **85**, 11E424 (2014).

[16] K. Kawahata, K. Tanaka, Y. Ito, A. Ejiri, and S. Okajima, Review of Scientific Instruments **70**, 707 (1999).

[17] S. Hirshman and W. van Rig, Computer Physics Communications **43**, 143 (1986).

[18] S. Lazerson, D. Gates, D. Monticello, H. Neilson, N. Pomphrey, A. Reiman, S. Sakakibara, and Y. Suzuki, in *Europhysics Conference Abstracts*, Vol. 35G (2011) p. O5.417, 38th EPS Conference on Plasma Physics.

[19] S. Lazerson and the DIII-D Team, Nuclear Fusion **55**, 023009 (2015).

[20] J. Huba, *NRL Plasma Formulary* (Naval Research Laboratory, 2013).

[21] S. Kubo, H. Idei, T. Shimozuma, Y. Yoshimura, T. Notake, K. Ohkubo, S. Inagaki, Y. Nagayama, K. Narihara, and The Lhd Experiment Group, J. Plasma Fusion Res. SERIES **5**, 584 (2002).

[22] S. Kubo, H. Idei, T. Shimozuma, Y. Yoshimura, T. Notake, K. Ohkubo, S. Inagaki, Y. Nagayama, K. Narihara, I. Yamada, S. Muto, S. Morita, and L. E. Group (LHD Experimental Group), AIP Conference Proceedings **669**, 187 (2003).

[23] C. D. Beidler and W. D. D'haeseleer, Plasma Physics and Controlled Fusion **37**, 463 (1995).

[24] C. D. Beidler and H. Maaßberg, Plasma Physics and Controlled Fusion **43**, 1131 (2001).

[25] S. Satake, M. Okamoto, N. Nakajima, H. Sugama, M. Yokoyama, and C. Beidler, Nuclear Fusion **45**, 1362 (2005).

[26] S. Matsuoka, S. Satake, M. Yokoyama, A. Wakasa, and S. Murakami, Physics of Plasmas **18**, 032511 (2011).

[27] C. Beidler, K. Allmaier, M. Isaev, S. Kasilov, W. Kernbichler, G. Leitold, H. Maaßberg, D. Mikkelsen, S. Murakami, M. Schmidt, D. Spong, V. Tribaldos, and A. Wakasa, Nuclear Fusion **51**, 076001 (2011).

[28] K. Ida, Plasma Physics and Controlled Fusion **40**, 1429 (1998).

[29] J. D. Callen, A. J. Cole, and C. C. Hegna, Physics of Plasmas (1994-present) **16**, 082504 (2009).

[30] H. Ehmler, J. Baldzuhn, K. McCormick, A. Kreter, T. Klinger, and W.-A. Team, Plasma Physics and Controlled Fusion **45**, 53 (2003).

PPPL PRINCETON PLASMA PHYSICS LABORATORY

Princeton Plasma Physics Laboratory
Office of Reports and Publications

Managed by
Princeton University

under contract with the
U.S. Department of Energy
(DE-AC02-09CH11466)

P.O. Box 451, Princeton, NJ 08543
Phone: 609-243-2245
Fax: 609-243-2751

E-mail: publications@pppl.gov

Website: http://www.pppl.gov